Supporting Information for

Dichotomy between frustrated local spins and conjugated electrons in a two-dimensional metal-organic framework

Wei Jiang,[a,b] Zheng Liu,*[,c] Jia-Wei Mei,*[,d] Bin Cui,[e] Feng Liu*[,a]

[a]Department of Materials Science and Engineering, University of Utah, Salt Lake City, UT 84112, USA
[b]Department of Electrical and Computer Engineering, University of Minnesota, Minneapolis, Minnesota 55455, USA
[c]Institute for Advanced Study, Tsinghua University, Beijing 100084, China
[d]Institute for Quantum Science and Engineering, and Department of Physics, Southern University of Science and Technology, Shenzhen 518055, China
[e]School of Physics, Shandong University, Jinan 250100, China

*E-mail: zheng-liu@mail.tsinghua.edu.cn; meijw@sustc.edu.cn; fliu@eng.utah.edu.

This PDF file includes:

Computational details
Electron filling and band formation
Band composition
Mott-Hubbard insulating physics
Competition between AFM and FM interaction
Simulations of spin-polarized STM/STS
Figs. S1 to S4
Tables S1 and S2
References

Computational details

The properties of HAB and Cu-$(HAB)_2$ molecules and $Cu_3(HAB)_2$ crystal are calculated using first-principles methods based on density functional theory (DFT). The molecular properties of HAB and Cu-$(HAB)_2$ were calculated using Gaussian package[1] with the B3LYP functional[2] and DFT method. For DFT calculations, we used the version 5.3 of the Vienna ab initio simulation package code[3]. Both the projected augmented wave[4,5] with the generalized gradient approximation (GGA)[6] and local density approximation (LDA) exchange-correlation potential methods were applied. The calculations were performed with a plane wave cutoff energy of 500 eV. The geometric optimizations were carried out without any constraint until the force on each atom is less than 0.01 eV $Å^{-1}$ and the change of total energy per cell is smaller than 10^{-4} eV.

For monolayer crystalline $Cu_3(HAB)_2$ calculation, the Brillouin zone K-mesh sampling was set as $15\times15\times1$. To eliminate the interaction between layers along the z direction, we introduced a vacuum layer with thickness of 15 Å. The lattice constant a was relaxed to be 13.645 Å. We first calculated the electronic properties without considering spin polarization, then both FM and 120° AFM spin configurations were studied considering spin polarization using the non-collinear method embedded in the VASP code. To better describe the localized $3d$ electrons of Cu, an additional on-site Hubbard U term is added in calculations. Different U values were tested. We further calculated bilayer system, using the same lattice constant a with a vacuum layer with thickness of 15 Å. Both A-A and A-B layer stacking is studied, which shows similar electronic properties as monolayer $Cu_3(HAB)_2$ because of the very week interlayer coupling.

To analyze the formation of different sets of bands, we have calculated band-resolved partial charge density and the maximally localized Wannier functions (MLWFs) to fit to the DFT band structures using the Wannier90 package[7]. Then, the results are compared with the molecular orbitals of the Cu-$(HAB)_2$ complex calculated using Gaussian. The scanning tunneling spectroscopy (STS) and spin-polarized STS (SP-STS) results were simulated by calculating the projected density of states around the Fermi level. The scanning tunneling microscopy (STM) topographies were simulated by calculating the energy-resolved partial charge density around different peaks of the dI/dV curve.

Electron filling and band formation

The coexistence and competition of local and itinerant electrons is one of the most fascinating problems in condensed matter physics. These interesting phases depend on a delicate balance of electron filling, $i.e.$, number of electrons on strongly-correlated heavy metals versus that on light-elements with strong π itinerancy. For crystalline $Cu_3(HAB)_2$, the d^9 electronic configuration of Cu^{2+} ion leads to an ideal half-filled Hubbard system, while the π bands are partially filled forming bands crossing the Fermi level. It is instructive to figure out the evolution of electron filling when organic molecules and metal ions form a crystal step-by-step, which will facilitate the design procedures to discover new systems that possess similar features.

Figure S1 shows the change of electron filling from single HAB molecule to Cu-$(HAB)_2$ complex to $Cu_3(HAB)_2$ crystal. For single HAB molecule, 12 unhybridized p_z orbitals from C and N form 12 π molecular orbitals (MO), in which 9 MOs are filled with 18 valence electrons. The three highest occupied MOs (HOMO) shows p_x, p_y, and p_z symmetries, which are denoted as π_x, π_y, and π_z. It is worth mentioning that π_x and π_y are energetically degenerated and have about 1.7eV energy difference compared to π_z MO [Fig. S1(a)]. It is also worth mentioning that we noticed that the four-coordinated Cu ions are not in the high symmetry positions as represented by different N-Cu-N angles along different directions. The 2nd order Jahn-Teller effect is also negligible as the energy splitting between different d orbitals is not small, which does not provide "pseudo-degenerate" d-orbital states.

When two HAB molecules are coordinated with one Cu ion through four Cu-N bonds, Cu donates two electrons to the neighboring N atoms forming d^9 electronic configuration. With a local square crystal field, the five degenerated d orbitals are split leaving the d_{xy} orbital half filled [Fig. S1(b)]. Thus, an ideal half-filled kagome band is formed by the Cu ions on the kagome lattice. On the other hand, when forming the Cu-$(HAB)_2$ complex, the left and right HAB MOs ($\pi^{L,R}$) form new bonding (π^L+π^R) and anti-bonding (π^L-π^R) MOs. Meanwhile, each HAB molecular unit receives one electron from Cu while loses two electrons by losing two hydrogen atoms. This leads to one electron loss and the half-filled anti-bonding MOs [Fig. S1(b)]. Further, in forming a crystalline $Cu_3(HAB)_2$, four more π electrons are lost while introducing two extra d^9 Cu^{2+} ions per unit cell. Therefore, the crystal bands ($p_{x,y}$ four bands)

formed by these π MO bases become one-fourth filled with their band dispersion determined by the energy difference between bonding and antibonding MOs. Meanwhile, the fully filled π_z MOs form an ideal graphene-like Dirac bands on the honeycomb lattice, which are about 1.7eV below the $p_{x,y}$ four bands [Fig. S1(c)].

Band composition

To further clarify our statement about formation of crystal band structure, we first calculated the band structure without considering the spin polarization and fitted using the wannier function. As shown in Fig. S2(a), the wannier fitted band structure is consistent with the schematic bands in Fig. S1(c) and the DFT calculated bands. Further, we calculated the band-resolved partial charge distribution and MLWFs, to be compared with the MOs calculated for Cu-$(HAB)_2$ complex from Gaussian. As shown in the Fig. S2(b), for the upper and lower Dirac bands, the partial charge distribution (left panel) show the same features as the bonding and anti-bonding MOs formed by HAB π_z MO (right panel). The upper Dirac/anti-bonding MO shows the hybridization feature between d_{xz} and π MOs. Moreover, the band dispersion of the Dirac band (0.8eV) is close to the energy difference between bonding and anti-bonding MOs (0.7eV). Similarly, as can be seen from Fig. S2(c), for the $\pi_{x,y}$ four bands, the partial charge distribution (left panel), MLWFs (middle panel), and the bonding and antibonding MOs (right panel) formed by π_x and π_y MOs consistent with each other perfectly. We find that only d_{xz} and d_{yz} orbitals are allowed to hybridize with π MOs formed by p_z orbitals because of the orbital symmetry.

Figure S2(d) shows the partial charge distribution of the kagome band, exhibiting the same shape of d_{xy} orbital. The charge is mainly located on the Cu ions with strong σ-antibonding to the neighboring N $p_{x,y}$ orbitals, which is identical to the calculated MOs and MLWFs [Fig. S2(d)]. The consistency between the band-resolved partial charge distribution and the MOs validates our approach of mapping MOs into the crystal band structure. This approach provides an effective bottom-up method to design materials with band structures of interest.

Mott-Hubbard insulating physics

It is important to specify whether the Cu spin-1/2 kagome system is a charge-transfer insulator or Mott-Hubbard insulator. First we noticed that there is no charge transfer between Cu d_{xy} orbital and conjugated-$\pi_{x,y}$ molecular orbitals of HAB. Such charge transfer is absent because of the vanishing orbital overlap $\langle d_{xy}|\pi_{x,y}\rangle = 0$ due to the reflection symmetry over the planar crystalline symmetry. On the other hand, the charge transfer between the symmetry-matched $p_{x,y}$ atomic orbitals of C, N and d_{xy} orbital of Cu is also minimal. It is because the $p_{x,y}$ atomic orbitals of C, N are located deep below the Fermi level (-9eV) far away from the d_{xy} orbital around the Fermi level, as displayed in Fig. S3. Therefore, considering the hopping between Cu ions in forming kagome bands, $Cu_3(HAB)_2$ contains an ideal Mott-Hubbard physics with anti-ferromagnetic (AFM) coupled Cu kagome system.

Competition between AFM and FM interaction

Considering the hopping between Cu ions, the half-filled spin-1/2 Hubbard Mott model yields an AFM exchange coupling between local spins, which can be described by a simplified Heisenberg model $H_d = J_d \sum_{\langle ij\rangle} \overrightarrow{S}_i \cdot \overrightarrow{S}_j$. $J_d = \frac{4t_d^2}{\tilde{U}}$ denotes the strength of the AFM coupling between Cu (d^9) local spins on the frustrated kagome lattice, which is determined by the hopping t_d and the on-site Hubbard repulsion $\tilde{U}$. On the other hand, the frustrated π electrons described by H_π prefer to have an FM coupling according to the Stoner's criteria. The FM coupling strength is determined by the number of π electrons on the flat band. Due to the Hund's coupling J_H between them, the overall spin configuration of $Cu_3(HAB)_2$ crystal depends on the relative strength of these two magnetic interactions. We note that $\tilde{U}$ value (Mott gap) varies with different U values (larger U values yield larger Mott gap) chosen for the LDA+U calculations. This could serve as an effective approach to artificially modify the AFM coupling strength (J_d) to examine the accuracy of our bi-frustrated spin-fermion model. As summarized in table S1, we calculated the energy difference between two spin configurations with different on-site U values. The FM spin configuration has all the spins aligned parallel with only FM exchange coupling, while the other one (named FR) has one spin direction flipped opposite to the other two spins containing both FM and AFM contributions. It is clear that the system with AFM

coupling has relatively lower energy with all the different on-site U values. In the meantime, with the decreasing of the on-site U value, the AFM coupling strength between Cu^{2+} local spins becomes stronger, as evidenced by the increasing energy difference between the two spin configurations. This is consistent with $J_d = \frac{4t_d^2}{\tilde{U}}$, in which the strength of AFM coupling is inversely proportional to the $\tilde{U}$.

Additionally, we can also tune the strength of the FM coupling of the frustrated π electrons by doping through either gating or chemical redox control method, which is experimentally feasible. More interestingly, due to the close energy proximity of the two subsystems, the system can be readily tuned into a series of unusual quantum states with different electron fillings. Therefore, we have also calculated the energy difference between FM and FR spin configurations as a function of π electron filling of $Cu_3(HAB)_2$ with an effective U value of 5 eV using LDA+U method.

As summarized in table S2, the dominating magnetism changes with different π electron fillings. When all the π electrons are removed (corresponding to zero π electron in table S2), the system is at the H_d side in the KAFM state, which is known to give rise to quantum spin liquid state. After adding the H_π^0 term by doping a small amount of π electrons (smaller than 0.5), the AFM coupling still dominates. These fractional fermions could peacefully coexist with AFM frustrated fermions, forming together a "fractional Fermi liquid" phase. Further, with more π electrons added in the system (less than 1.5), the flat-band ferromagnetism dominates due to the Stoner's criteria with the large-DOS limit. Moreover, because of the strong Hund's coupling between Cu local spins and the itinerant electrons, the KAFM subsystem is also polarized into a FM configuration, leading to a FM phase. When further increasing the number of π electrons (larger than 1.7), the spin-polarization of the π electrons decreases leading to a weaker FM coupling. Then the AFM magnetism dominates and the system returns to a Fermi liquid phase, which is consistent with the energy difference calculation shown in table S2 for the intrinsic case (2 π electrons). Based on these results, we draw a phase diagram with the evolution of quantum phases as a function of electron filling and correlation strength, as shown in Fig. 1(c) in the main text. Similarly, we find the AFM coupling is greatly enhanced with smaller on-site U values while the FM phase is strongly suppressed, as shown in the phase diagram in Fig. 1(c). We have also calculated the system using GGA+U in comparison with that from LDA+U. The

results show that with the same U value, GGA+U tends to amplify the FM state than LDA+U, as shown in table. S2.

Simulations of spin-polarized STM/STS

Distinct from traditional inorganic dichotomy systems, the dichotomy feature of two-dimensional (2D) MOF can be directed monitored through either scanning tunneling microscopy/spectroscopy (STM/STS) or the cutting-edge spin-polarized STM/STS. Here, using the KAFM state as an example [Fig. S4(a)], we demonstrate how different spin configurations can be directly distinguished through SP-STM. Without π electrons, the system is regarded as an ideal S-1/2 AFM QSL state. People propose that 120° AFM spin configuration represents the magnetic state with the lowest energy. Consequently, for that phase, the SP-STS measurements produce the same results for both spin channels. As shown in Fig. S4(b), lower and upper Hubbard peaks can be clearly seen below and above the Fermi level. Under strong magnetic field, all the local spins become parallelized. Therefore, we get two distinct STS results for two spins, as shown by blue and red curved in Fig. S4(c), respectively. For both spin configurations, the system remains in the insulating state, representing either a Mott insulator or an FM insulator.

Further, we are going to demonstrate that SP-STM/STS can be used to explore dichotomy physics on this special 2D MOF platform. We show that not only the dichotomy feature can be directly identified, but also the connection between the magnetism and exotic quantum phenomena can be built, such as between the formation of magnetic polaron and giant magnetoresistence (GMR) effect. Firstly, the dichotomy feature can be directly identified using simple STS measurements, where lower/upper Hubbard peak is prominent below/above the Fermi level. The itinerant electrons locate right at the Fermi level, as shown in Fig. S4(e). With STM topographies measured around these characteristic voltage regions, bi-frustrated localized spin and itinerant electrons can be further identified, as we demonstrated in the main text (Fig. 4).

The GMR effect in dichotomy system has been well documented. Figure S4(d) shows the formation of magnetic polaron under the AFM background due to strong Hund's coupling between local spins and itinerant electrons. Applying strong magnetic field, all the local spins aligned parallel. This causes the annihilation of magnetic polaron and leads to the ferromag-

netic metallic state. With different spin configurations between magnetic polaron and FM state, SP-STS/STM can be applied to distinguish the two states by identifying the spin degree of freedom. As shown in Fig. S4(f), the SP-STS simulation results for FM $Cu_3(HAB)_2$ can clearly distinguish two spin channels. States coming from Cu ions are fully spin-polarized with different spins located below and above the Fermi level, respectively. States from organic ligands are also spin polarized with the same spin splitting direction as the localized spins, indicating strong ferromagnetic coupling between the two.

The magnetic polaron is essentially an FM cluster embedded within the AFM spin background. Therefore, SP-STS results above the magnetic polaron region should reproduce similar spectra as FM spin configuration [Fig. S4(f)]. Differently, SP-STS results above the AFM spin background area should reproduce spectra as Fig. S4(c). Applying strong magnetic field, the SP-STS results would show features of FM metal as Fig. S4(f). Combining with the conductivity measurements with and without the strong magnetic field, direct connection can be built between the formation of magnetic polaron and GMR effect. The aforementioned method can also be used to directly monitor the phase evolution as shown in Fig. S4(a), as different phases possess distinct spin configurations. Therefore, we conclude that 2D MOFs provide an exciting and versatile platform to further explore dichotomy physics, which has been found rather difficult in traditional inorganic dichotomy systems.

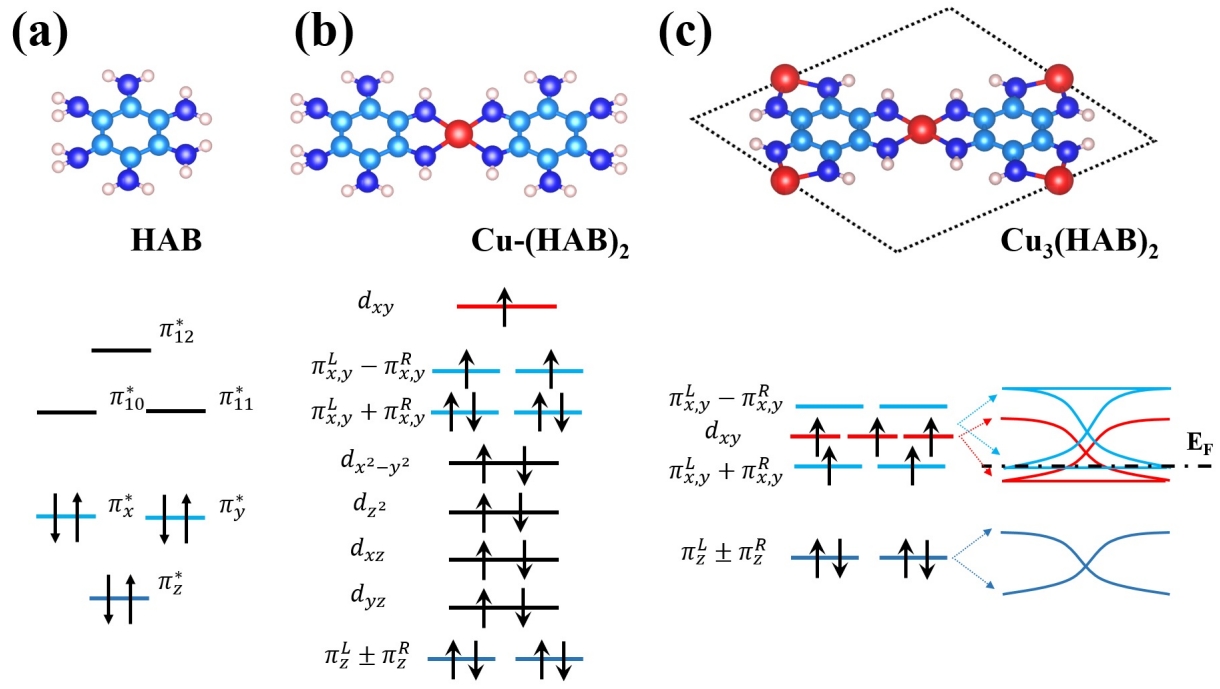

Fig. S1. Change of the electron filling when HAB molecule forms $Cu_3(HAB)_2$ crystal.. (a) and (b) Frontier molecular orbital diagram of molecular HAB and Cu-$(HAB)_2$ complex. (c) Schematic band diagram formed by the overlap of molecular orbitals from HAB and d orbitals from Cu.

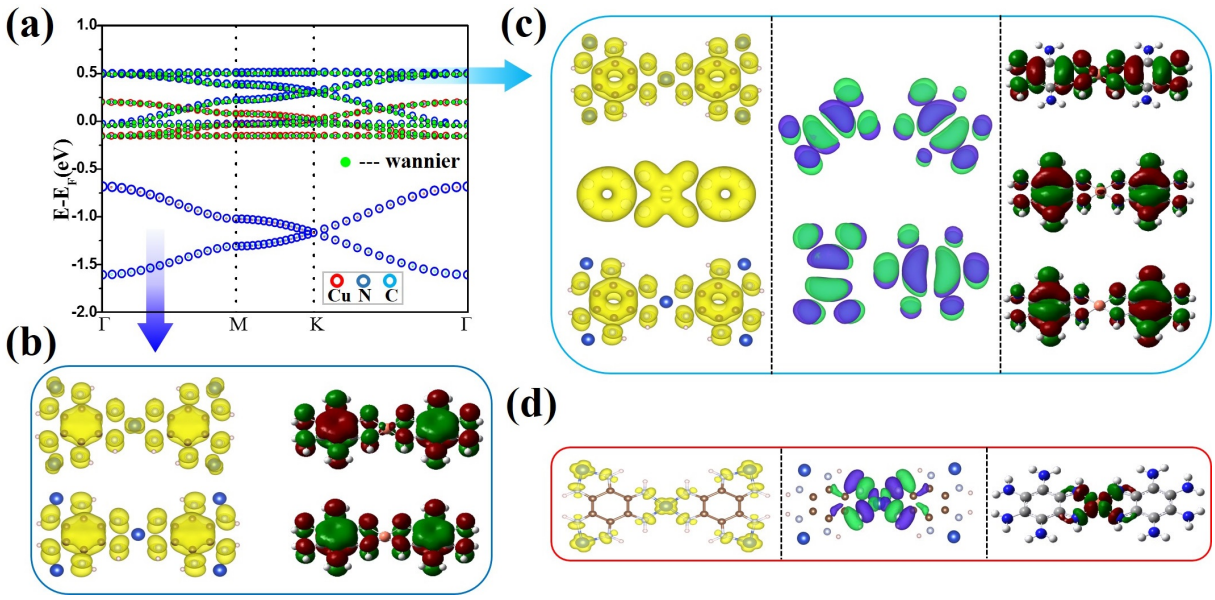

Fig. S2. Band composition. (a) Calculated band structure along high-symmetry K-path. Green dotted lines are the wannier fitted band structure. (b) The partial charge distributions (left panel) calculated for the Dirac bands, which show the same feature as their corresponding MOs formed by π electrons (right panel). (c) and (d) The partial charge distributions (left panel) and MLWFs (middle panel) calculated for the four bands and kagome bands, respectively, showing the same shape as MOs of Cu-$(HAB)_2$ complex (right panel).

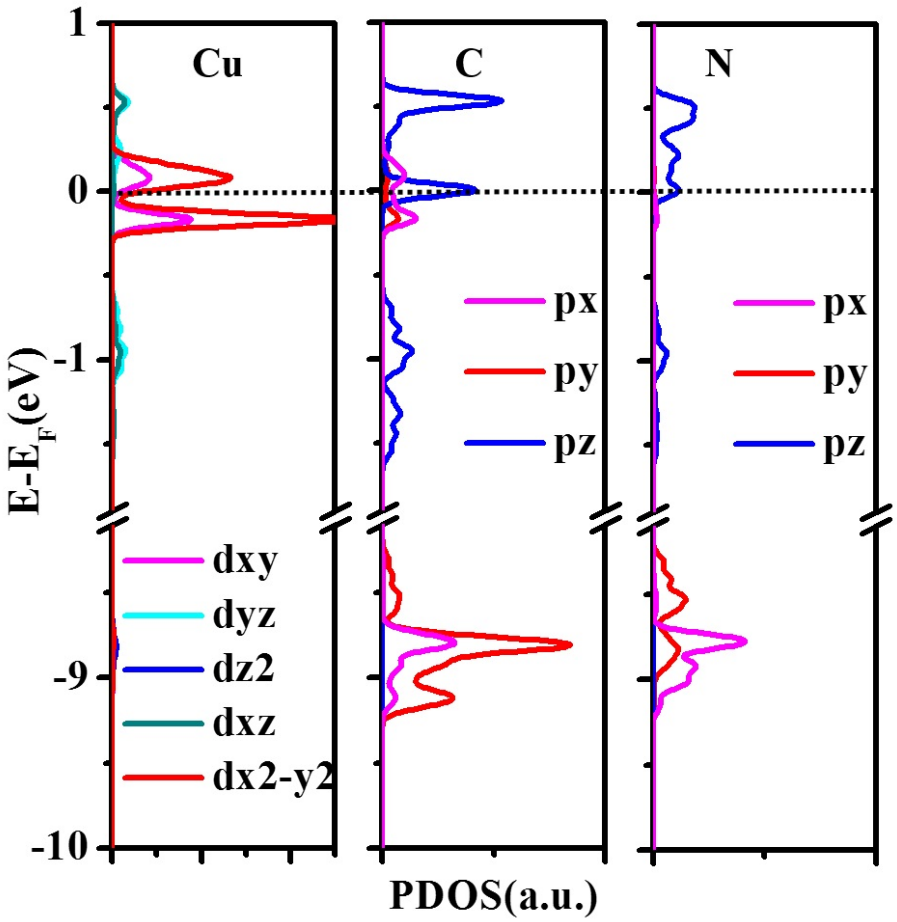

Fig. S3. Orbital-resolved density of states for $Cu_3(HAB)_2$ crystal.

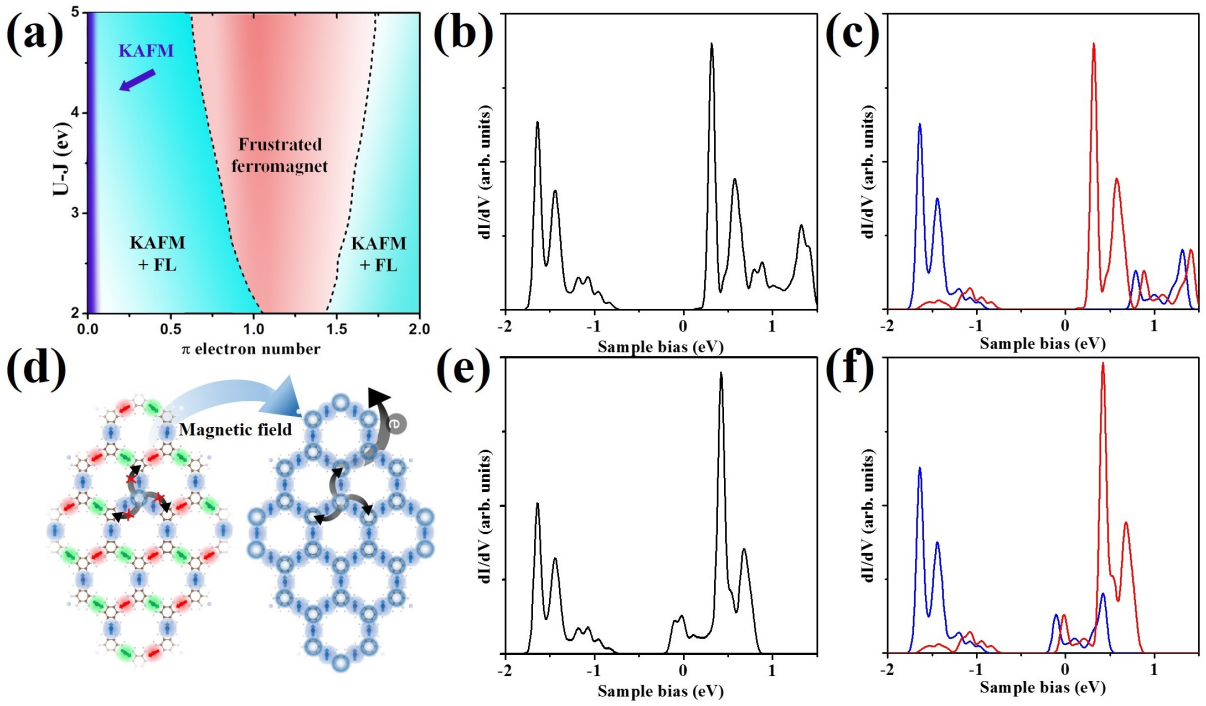

Fig. S4. SP-STM/STS simulation. (a) Phase diagram versus on-site U term and the electron filling. SP-STS simulations for KAFM state without π electrons in (b) 120° AFM spin configuration and (c) FM spin configuration. (d) Formation of magnetic polaron under kagome AFM background and FM spin configuration under magnetic field. SP-STS simulations for dichotomy system with coexistence of local spins and itinerant electrons in (e) AFM spin configuration and (f) FM spin configuration. Black curves indicate same STS results for both spin channels, and red and blue curves indicate STS results for spin-up and spin-down states, respectively. Each spectrum shown here represent an averaged results for a certain area.

Table S1. The energy difference $\triangle$E between FM and FR (E_{FR}-E_{FM}) spin configurations with different on-site U values.

U-J (eV)	2	3	4	5
$\triangle$E (meV)	-16.6	-13.0	-10.4	-8.6

Table S2. Phase evolution as a function of π electron filling of $Cu_3(HAB)_2$ crystal with an effective U value of 5eV. $\triangle E$ = E_{FR}-E_{FM} with positive values indicating preference of FM coupling.

π electrons #	0	0.5	0.75	1	1.5	1.7	2	2.1
LDA+U $\triangle$E (meV)	-10.0	-1.8	2.6	5.7	6.5	-0.7	-8.6	-10.1
GGA+U $\triangle$E (meV)	-8.3	-1.7	1.5	4.5	11.2	15.7	19.8	-8.1

References

(1). Andzelm J., Wimmer E. *The Journal of Chemical Physics* **1992**, 96, 1280.

(2). Stephens P.J., Devlin F.J., Chabalowski C.F., Frisch M.J. *J. Phys. Chem.* **1994**, 98, 11623.

(3). Kresse G., Hafner J. *Phys. Rev. B* **1993**, 47, 558.

(4). Blöchl P.E. *Phys. Rev. B* **1994**, 50, 17953.

(5). Kresse G., Joubert D. *Phys. Rev. B* **1999**, 59, 1758.

(6). Perdew J.P., Burke K., Ernzerhof M. *Phys. Rev. Lett.* **1996**, 77, 3865.

(7). Mostofi A.A., et al. *Computer Physics Communications* **2008**, 178, 685.